







# High-speed super-resolution structured illumination microscopy with a large field-of-view

MENGDI GUO,<sup>1</sup> YUNHUA YAO,<sup>1,7</sup>  ZHENGQI HUANG,<sup>1</sup> YU HE,<sup>1</sup>  
BOZHANG CHENG,<sup>1</sup> DALONG QI,<sup>1</sup>  YUECHENG SHEN,<sup>1</sup>   
LIANZHONG DENG,<sup>1</sup> ZHIYONG WANG,<sup>2</sup> KEBIN SHI,<sup>3</sup> XIAOCONG  
YUAN,<sup>4</sup> ZHENRONG SUN,<sup>1</sup> AND SHIAN ZHANG<sup>1,5,6,8</sup> 

<sup>1</sup>State Key Laboratory of Precision Spectroscopy, School of Physics and Electronic Science, East China Normal University, Shanghai 200241, China

<sup>2</sup>School of Mathematical Sciences, University of Electronic Science and Technology of China, Chengdu 611731, China

<sup>3</sup>State Key Laboratory for Mesoscopic Physics, Department of Physics, Peking University, Beijing 100871, China

<sup>4</sup>Key Laboratory of Optoelectronic Devices and Systems of Ministry of Education and Guangdong Province, College of Physics and Optoelectronic Engineering, Shenzhen University, Shenzhen 518060, China

<sup>5</sup>Joint Research Center of Light Manipulation Science and Photonic Integrated Chip of East China Normal University and Shandong Normal University, East China Normal University, Shanghai 200241, China

<sup>6</sup>Collaborative Innovation Center of Extreme Optics, Shanxi University, Taiyuan 030006, China

<sup>7</sup>yhyao@lps.ecnu.edu.cn

<sup>8</sup>sazhang@phy.ecnu.edu.cn

**Abstract:** Structured illumination microscopy (SIM) has been extensively employed for observing subcellular structures and dynamics. However, achieving high-speed super-resolution SIM with a large field of view (FOV) remains challenging due to the trade-offs among spatial resolution, imaging speed and FOV under limited bandwidth constraints. Here, we report a novel SIM technique to address this issue. By utilizing a high-speed camera and a rolling image reconstruction strategy to accelerate super-resolution image acquisition, as well as using a deep resolution enhancement to further improve spatial resolution, this SIM technique achieves imaging with a spatial resolution of 94 nm, a FOV of  $102 \times 102 \mu\text{m}^2$ , and an imaging speed of 1333 frames per second. The exceptional imaging performance of this proposed SIM technique is experimentally demonstrated through the successful recording of the Brownian motion of fluorescent microspheres and the photobleaching of fluorescently labeled microtubules. This work offers a potential tool for the high-throughput observation of high-speed subcellular dynamics, which would bring significant applications in biomedical research.

© 2024 Optica Publishing Group under the terms of the [Optica Open Access Publishing Agreement](#)

## 1. Introduction

Super-resolution fluorescence microscopy, which surpasses the spatial resolution limitation of conventional microscopy, has been an essential tool for studying intricate subcellular structures and dynamics [1,2]. Prominent techniques include stimulated emission depletion microscopy (STED) [3,4], which enhances resolution by shrinking the point spread function (PSF) with nonlinear stimulated emission depletion; single molecule localization microscopy (SMLM) [5,6], which achieves higher resolution by localizing single fluorescent molecules with sparse activation rather than recording fluorescence distribution; and structured illumination microscopy (SIM) [7,8], which encodes normally inaccessible high-resolution information into observed images using the moiré effect. In recent years, super-resolution fluorescence microscopy techniques have been rapidly advanced. Notably, improvements in spatial resolution and imaging speed

have significantly expanded the ability to observe fine structures and dynamics. For instance, by scanning a doughnut-shaped excitation spot and probing the fluorophore with a local intensity minimum, molecule localization with minimal emission fluxes (MINFLUX) minimizes the number of fluorescence photons required for high localization precision, achieving a spatial resolution of 6 nm [9]. Similarly, minimal STED (MINSTED) utilizes a STED doughnut to narrow the effective PSF and searches for the doughnut position with minimal STED [10]. Combining with photoswitching fluorophores, MINSTED achieves a spatial resolution down to 2 nm with reduced fluorophore bleaching and background noise. Moreover, Ångström-resolution is achieved through a DNA-barcoding method, named resolution enhancement by sequential imaging (RESI) [11]. RESI uses orthogonal DNA barcodes combined with imaging and washing cycles to enable sequential target multiplexing. By increasing the localization times for a single target, RESI greatly improves the spatial resolution. Despite the high spatial resolution offered by these localization-based super-resolution microscopy techniques, it is often challenging for them to observe subcellular dynamics due to the time-consuming nature of point scanning or multiple measurements.

Alternatively, SIM serves as an outstanding tool for super-resolution imaging of dynamics in live cells due to its high imaging speed, low excitation power, and broad applicability of fluorescent labels. In terms of spatial resolution, linear SIM only achieves a two-fold resolution improvement, because the structured illumination patterns are diffraction-limited by the objective lens. Nonlinear SIM, which leverages fluorescence saturation [12] or reversible photoswitching [13], can significantly enhance spatial resolution, but it suffers from severe photobleaching and increased acquisition time, making it less desirable. Recently, computation-based resolution enhancement methods have been adopted to further increase the spatial resolution of SIM without hardware modification. By exploiting the sparsity and continuity of biological structures, the sparse deconvolution algorithm further increased the resolution of SIM by nearly twofold [14]. Untrained neural networks were also employed to perform deconvolution by leveraging the implicit priors in the network, thus eliminating the need for meticulous artificial parameter optimization [15,16]. Regarding imaging speed, SIM surpasses other super-resolution techniques because it requires only a few images for reconstruction. However, the final imaging speed of SIM is still constrained by the image acquisition speed of the camera. Several strategies have been proposed to break this limitation. For example, the number of frames needed for SIM reconstruction can be reduced from 9 to 4 by utilizing the redundancy information in the images captured under various illumination patterns. Various methods such as the Bayesian framework [17], least squares method [18], modified incoherent Fourier ptychographic procedure [19] and maximum likelihood approach [20] have been employed to handle image reconstruction with fewer frames. Additionally, compressed imaging-based SIM accelerated super-resolution imaging by compressing several illuminated images into a single image and then recovering the super-resolution image from the compressed data [21,22]. Moreover, by combining enhanced temporal compressive microscopy with deep-learning-based super-resolution image reconstruction, temporal compressive super-resolution microscopy (TCSR) achieved high-speed super-resolution imaging with a frame rate of 1200 frames per second (fps) and a spatial resolution of 100 nm [23]. However, the field of view (FOV) is limited, and the image reconstruction in TCSR relies on the motion estimation of the target, which restricts its application scenarios. Given the finite pixel count of an image sensor, the upper limiting spatial resolution and FOV size of a microscope system are inherently in conflict. Typically, a higher spatial resolution results in a smaller FOV, particularly in super-resolution microscopy [24]. Image stitching through scanning imaging [25] or secondary imaging with multiple cameras [26] can enlarge the FOV while maintaining spatial resolution, but these methods significantly reduce imaging speed and impose stringent requirements for system construction and calibration. Additionally, high-speed imaging with high spatial resolution and a large FOV necessitates data collection and storage with a large bandwidth, which is challenging

for conventional cameras to achieve. Therefore, realizing high-speed super-resolution imaging with a large FOV remains a significant challenge.

In order to simultaneously achieve the high-speed, large-FOV and super-resolution imaging, here we develop a novel SIM technique. By employing a high-speed camera and a rolling image reconstruction strategy, the super-resolution imaging speed is significantly improved. Meanwhile, the high spatiotemporal bandwidth of the high-speed camera due to special electronics design also allows for a high FOV associated with the high imaging speed [27]. By further improving the spatial resolution with a deep resolution enhancement, the novel SIM technique achieves imaging with a spatial resolution of 94 nm, an imaging speed of 1333 fps and a FOV of  $102 \times 102 \mu\text{m}^2$ . The high-speed, large-FOV and super-resolution imaging ability is experimentally validated by observing the Brownian motion of fluorescent microspheres and the photobleaching of fluorescently labeled microtubules in NIH/3T3 cells. This proposed SIM technique provides a well-established tool for the high-throughput observation of rapid subcellular dynamics, which will have great application prospects in biomedical imaging.

## 2. Methods

The experimental setup of the proposed SIM technique is illustrated in Fig. 1(a). The laser emitted from a continuous wave (CW) laser with a wavelength of 532 nm (Laser Quantum, Torus 532) is expanded by a beam expander (BE, Daheng Optics, GCO-2501) and then modulated by a digital micromirror device (DMD, Texas Instruments, DLP6500), which is used to load stripe patterns with three directions and three steps of phase shift. After passing through a 4f imaging system comprising a pair of lenses (L1 and L2), the modulated laser is relayed to an objective lens (OL, Olympus, UPLAPO100XOHR) with a magnification of 100 $\times$  and NA of 1.5, and then projected onto the sample. Here, a structured illumination is formed by interference. A spatial filter (SF) in the Fourier plane of the 4f imaging system is utilized to isolate the diffracted light of  $\pm 1$  levels and block the diffracted light of other levels. The fluorescence emitted from the sample is collected by the same objective lens, transmitted through a dichroic mirror (DM, CHROMA, ZT532rdc), a filter (F1, Thorlabs, FGL550S) and a 2 $\times$  tube lens (TL), and ultimately captured by a high-speed camera (Photron, FASTCAM NOVA S6) with an image magnification of 200 $\times$ . The polarization modulation module, which is composed of a quarter-wave plate (QWP, Lbtek, MQWP20-532BM), a linear polarizer (LP, Thorlabs, LPVISA100-MP2), a half-wave plate (HWP, Thorlabs, WPH10M-532), and a customized pizza half-wave plate (PHP, Lbtek, AHWP25-VIS-A-6P-M), is designed to enhance the contrast of structured illumination on the sample by aligning the polarization direction of the laser beam with the orientation of the fringes. The high-speed camera is triggered by the output signal of the DMD for synchronization.

The flowchart of the image reconstruction is shown in Fig. 1(b). The raw SIM images captured by the high-speed camera are processed sequentially to generate the super-resolution image sequence. The photon number is limited due to the short exposure time at high imaging speeds, leading to a restricted signal-to-noise ratio (SNR) in the raw images. A high-fidelity structured illumination microscopy (HiFi-SIM) algorithm is used to conduct the SIM reconstruction, which offers the advantages of high fidelity and low artifacts through point-spread-function engineering [28]. Moreover, a rolling reconstruction strategy is utilized to process the image sequence [29]. Every 9 adjacent frames are used to obtain a super-resolution image with an interval of 3 frames instead of 9 frames. By employing this method, the speed of super-resolution imaging can be tripled. To further improve the spatial resolution while maintaining imaging speed, deep resolution-enhanced SIM (DRE-SIM) is utilized for additional post-processing of the SIM images. DRE-SIM combines the degradation model of the SIM system with an untrained neural network based on the concept of deep image prior [30], enabling further enhancement of image resolution [15,16]. In DRE-SIM, the input SIM image  $x_0$  is initially processed by a neural network with randomly initialized parameters  $\theta$ , the output image  $f_\theta(x_0)$  is then convolved with an equivalent

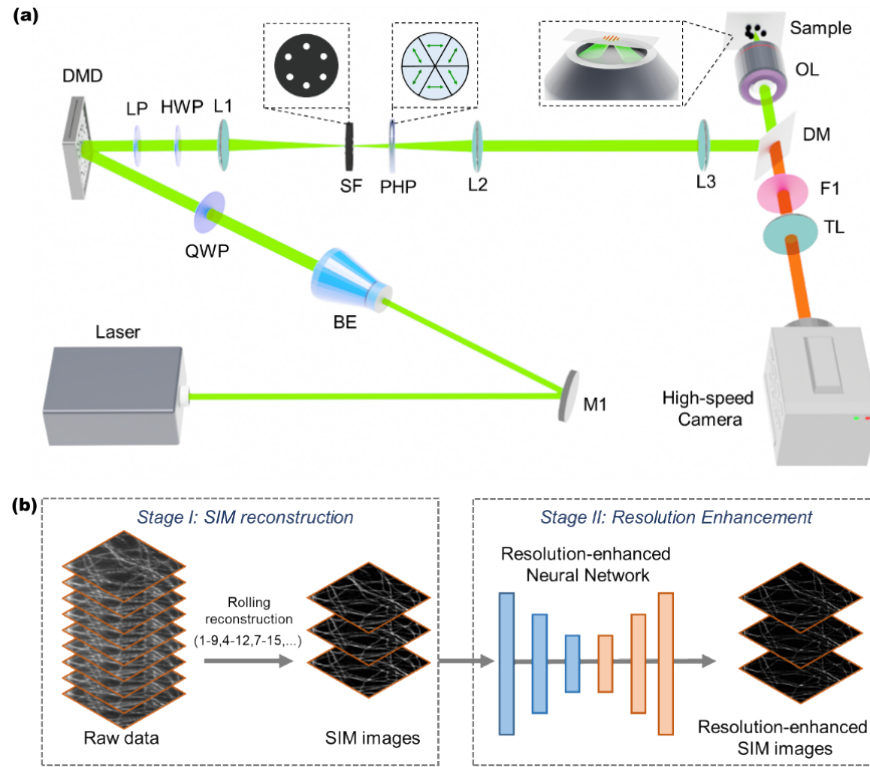


**Fig. 1.** Experimental setup and image reconstruction flow of the proposed SIM technique. (a) Experimental arrangement. M1: Mirror; BE: Beam expander; QWP: Quarter-wave plate; DMD: Digital micromirror device; LP: Linear polarizer; HWP: Half-wave plate; L1–L3: Lenses; SF: Spatial filter; PHP: Pizza half-wave plate; DM: Dichromatic mirror; OL: Objective lens; TL: Tube lens; F1: Spectral filter. (b) Image reconstruction flowchart based on SIM reconstruction and resolution enhancement.

PSF of SIM to acquire the corresponding SIM image  $O(f_{\theta}(x_0))$ . Here, the equivalent PSF of SIM is estimated based on the optical parameters of the SIM system, which includes the cut-off frequency bound of the microscope and the frequency shift of the structured illumination patterns. The loss function is iteratively calculated to update the neural network parameters  $\theta$ , and is given by

$$loss = \| O(f_{\theta}(x_0)) - x_0 \|_1 + \mu \| f_{\theta}(x_0) \|_{TV}, \quad (1)$$

where the first part is the fidelity term, which assesses the difference between the input SIM image and the calculated image following the SIM image formation model by L1 norm, and the second part is the total variation (TV) regularization term, which imposes constraints to reduce artifacts and noise. The weight parameter  $\mu$  is utilized to balance the fidelity and regularization term, requiring fine-tuning for samples with varying morphology or noise levels. After several iterations, the neural network can generate a resolution-enhanced image. The task of DRE-SIM can be considered as an optimization process aimed at finding the optimal parameters of a neural network to enhance the resolution of SIM images, which can be expressed by

$$x^* = f_{\theta^*}(x_0), \quad \theta^* = \arg \min_{\theta} loss(f_{\theta}(x_0), x_0), \quad (2)$$

where  $x^*$  is the resolution-enhanced image. DRE-SIM can further enhance the resolution based on SIM images, requiring minimal parameter optimizations and eliminating the necessity for training

datasets. Through the utilization of rolling SIM reconstruction and resolution enhancement techniques, a sequence of super-resolution images with high speed and spatial resolution is achieved.

### 3. Results and discussion

To maximize the FOV size of our SIM system, the pixel counts of the high-speed camera is set as the maximal value of  $1024 \times 1024$ . Given a pixel size of  $20 \mu\text{m}$  and an image magnification of  $200\times$ , the FOV is estimated to be approximately  $102 \times 102 \mu\text{m}^2$ . The frame rate of the high-speed camera at the pixel counts of  $1024 \times 1024$  can reach 6400 fps. However, considering the requirement of raw images with a sufficiently high SNR for SIM reconstruction, the frame rate of the high-speed camera is set at 4000 fps for all subsequent experiments, corresponding to an exposure time of 0.25 ms. It results in a super-resolution imaging speed of approximately 1333 fps with the rolling reconstruction strategy. To characterize the spatial resolution of the system, we first image static fluorescent microspheres with a diameter of 80 nm and an emission wavelength of 580 nm (Zhongke Keyou, ZKKY-PS-2-07-80). The laser power density is set as  $17.7 \text{ W/cm}^2$ . The acquired images are reconstructed using the HiFi-SIM algorithm and then subsequently processed with DRE-SIM for resolution enhancement. A selected frame from the results is depicted in Fig. 2(a). As the microspheres are relatively small within the FOV, enlarged views of certain regions have been included in the image. To exhibit the super-resolution performance, a region of interest highlighted with a yellow box in Fig. 2(a) is chosen and the corresponding wide-field (WF), SIM, and DRE-SIM images of this region are presented in Figs. 2(b)–2(d). It is evident that the size of the fluorescent microspheres treated by DRE-SIM is significantly smaller than those of the WF and SIM. For quantitative analysis of the resolution enhancement, the intensity distributions of the same fluorescent microsphere along the horizontal lines in WF, SIM, and DRE-SIM images are extracted, as depicted in Fig. 2(e). The full width at half maximum (FWHM) of the intensity profile is calculated to be 279 nm, 142 nm, and 94 nm, respectively. This analysis demonstrates that the proposed SIM technique can achieve a resolution of up to 94 nm.

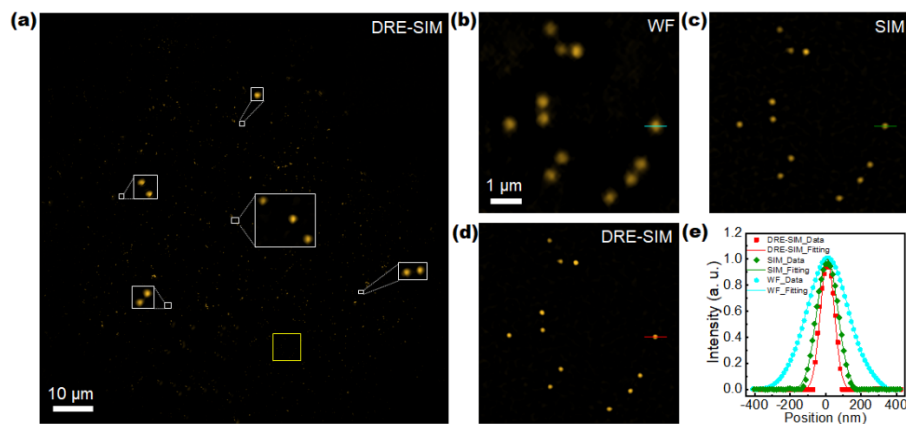


**Fig. 2.** Spatial resolution characterization of our SIM system by imaging fluorescent microspheres with a diameter of 80 nm. (a) The DRE-SIM image of fluorescent microspheres, here the insets labeled with white dash boxes show enlarged views of the selected regions. (b)–(d) WF, SIM, and DRE-SIM images of the region labeled with the yellow box in (a). (e) The intensity distributions of the same fluorescent microsphere along the labeled lines in the WF, SIM, and DRE-SIM images, together with the Gaussian fitting results.



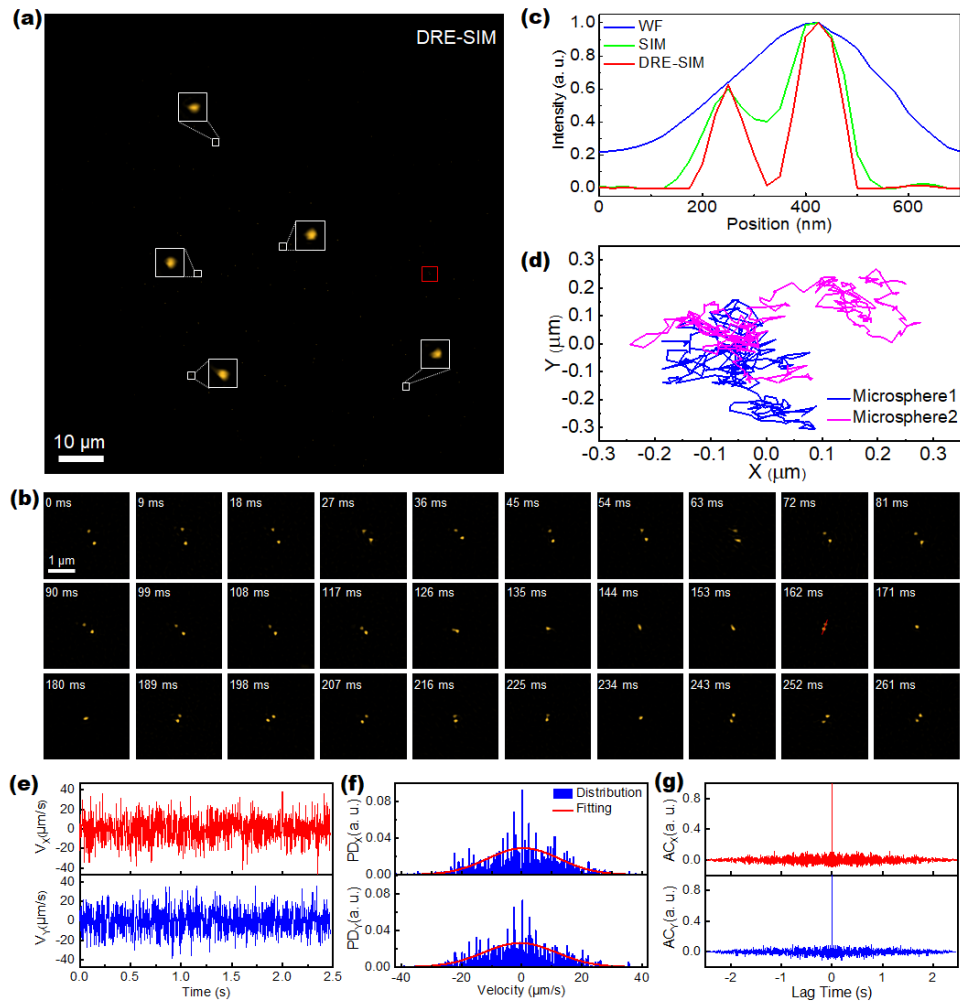


**Fig. 3.** Imaging the Brownian motion of fluorescent microspheres by our SIM system. (a) A DRE-SIM image of fluorescent microspheres, associated with five enlarged views of the regions labeled by white boxes. (b) 30 selected frames on the selected region labeled with a red box in (a). (c) Intensity distributions along the red labeled lines in WF, SIM and DRE-SIM images at 162 ms. (d) Trajectories of the two fluorescent microspheres in two-dimensional plane within the selected region labeled with a red box in (a). (e) Evolution of the velocity components in two orthogonal directions of a microsphere. (f) Probability densities of the two velocity components. (g) Autocorrelation coefficients of the two velocity components.

To verify the imaging capability of our SIM system, we observe the Brownian motion of fluorescent microspheres. Brownian motion, a classical physical phenomenon, entails the random movement of particles suspended in a medium, attributed to the asymmetric impacts of surrounding molecules [31,32]. This phenomenon indirectly reveals the random thermal motion of molecules, providing a platform for the study of statistical mechanics and thermodynamics [33,34]. A microscopic system with high speed, high resolution, and a large FOV offers an ideal tool for tracking a large number of particles, which is preferred for analyzing Brownian motion. Fluorescent microspheres (Thermofisher, F8800) with a diameter of 100 nm and an emission

wavelength of 560 nm are dispersed in ethylene glycol. The solution is dripped onto a cover glass and then covered with another cover glass. Finally, the sample is imaged by our system under the excitation of the 532 nm laser with a power density of  $17.7 \text{ W/cm}^2$ . A selected frame of the reconstructed images is shown in Fig. 3(a), along with an enlarged view of several fluorescent microspheres. To clearly demonstrate the Brownian motion of fluorescent microspheres, 30 frames with a 9 ms interval on the selected region marked with a red box are enlarged, as depicted in Fig. 3(b). The corresponding video is provided in [Visualization 1](#). It can be observed that two microspheres move randomly and are in close proximity in some frames. The intensity distributions of WF, SIM and DRE-SIM images along the red line at 162 ms are extracted and shown in Fig. 3(c). Additionally, the centroids of the two microspheres are extracted and presented in Fig. 3(d). While the two microspheres cannot be distinguished by WF microscope, our SIM technique enables their differentiation, highlighting the advantages of our approach in capturing Brownian motion. Based on the super-resolution image sequence, the temporal evolution of Brownian motion can be further analyzed. By extracting the motion of a single microsphere from 1100 super-resolution images within 2.5 seconds, we obtain the evolution of velocity components in two orthogonal directions, as shown in Fig. 3(e). The probability densities of the velocity components are calculated, demonstrating a Gaussian distribution with a mean of zero, as depicted in Fig. 3(f). The autocorrelation functions of the velocity components are also calculated as shown in Fig. 3(g). The low autocorrelation except at the lag time of zero indicates a weak memory effect in the velocity, reflecting the randomness of the microsphere's motion [31]. The diffusion coefficient is calculated based on the one-dimensional mean squared displacement extracted from the recorded images, which is approximately  $8.09 \times 10^{-14} \text{ m}^2/\text{s}$ . This value aligns well with the one calculated by the Stokes-Einstein equation [35], which is  $8.25 \times 10^{-14} \text{ m}^2/\text{s}$ . These results further confirm the reliability of our high-speed super-resolution imaging system.

To showcase the wide applicability of this SIM technique for high-speed super-resolution imaging of biological structures, we conduct experimental observations on the photobleaching of fluorescently labeled microtubules in NIH/3T3 cells. Microtubules are crucial structures in cells, playing important roles in maintaining cell morphology and participating in cell division, cell transport, and cell polarity. Photobleaching, characterized by the irreversible photochemical destruction of a fluorophore, poses challenges to most fluorescence microscopy techniques [36], which diminishes the SNR of acquired images and impedes the time-lapse tracking of fluorescent targets. Studying the kinetics of photobleaching aids in seeking methods to mitigate it [37,38]. In our experiment, the sample was purchased from Standard Imaging (Beijing) Biotechnology Co. Ltd. NIH/3T3 cells are incubated with beta-tubulin primary antibodies and Cy3b secondary antibodies for fluorescent labeling. A CW laser with a wavelength of 532 nm is used to continuously excite the sample with the power density of  $14.1 \text{ W/cm}^2$ , and 21821 frames are collected by our system, resulting in a super-resolution image sequence comprising 7273 frames with a time interval of 0.75 ms. The corresponding video is provided in [Visualization 2](#). A comparison of WF, SIM, and DRE-SIM images of one selected frame is presented in Fig. 4(a). The region labeled by the white box is enlarged to reveal fine details, and the corresponding WF, SIM, and DRE-SIM images are provided in Figs. 4(b)–4(d), respectively. Evidently, the resolution of the reconstructed images is further enhanced with DRE-SIM. The intensity distributions along three labeled lines are also extracted, as shown in Fig. 4(e). DRE-SIM can distinguish adjacent tubulin microtubules, which are challenging to distinguish even in SIM. The resolution of the WF, SIM, and DRE-SIM images is estimated by Fourier ring correlation [39] to be 258 nm, 131 nm, and 98 nm, respectively. This demonstrates the significant resolution improvement achieved by DRE-SIM. To determine the photobleaching kinetics under these conditions, the fluorescence intensity evolution within the selected region marked with a yellow box in Fig. 4(d) is extracted and shown in Fig. 4(f) along with the fitting curve generated by the biexponential method. The

effective bleaching rate constants are estimated to be 5.2 and 0.3 s, which reveals the time scales of the underlying processes in photobleaching. Our SIM technique offers a versatile tool for studying photobleaching kinetics in a large FOV with high frame rate and high spatial resolution.

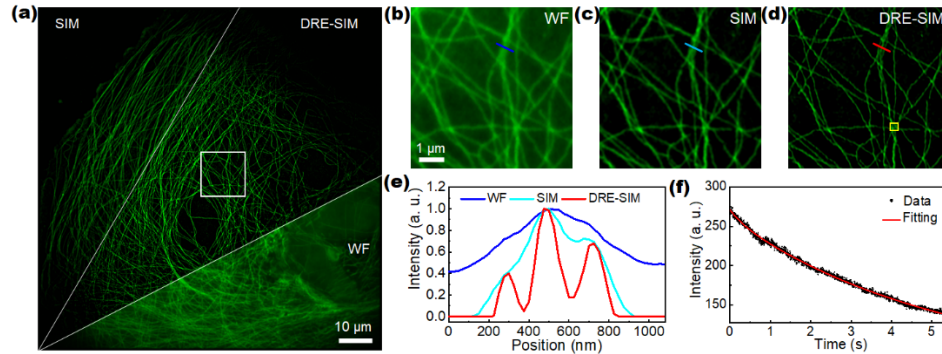


**Fig. 4.** Imaging the photobleaching of fluorescently labeled microtubules in NIH/3T3 cells by our SIM system. (a) SIM (top), DRE-SIM (middle) and WF (bottom) images of microtubules in NIH/3T3 cells. (b)-(d) Magnified views of WF, SIM, and DRE-SIM in the region marked by the white box in (a). (e) Intensity distributions along the labeled lines in the WF, SIM, and DRE-SIM images. (f) Fluorescence intensity decay curve in the region labeled with the yellow box in (d), associated with a biexponential decay fitting.

#### 4. Conclusions

In summary, we have developed a high-speed super-resolution SIM technique with a large FOV. This advancement is obtained through the large bandwidth image acquisition by a high-speed camera and a roll reconstruction strategy. Here, the large bandwidth allows a large FOV associated with a high imaging speed. The application of the deep resolution enhancement-based SIM algorithm further enhances the resolution of SIM images. Consequently, we achieved an excellent imaging ability with a spatial resolution of 94 nm, an imaging speed of 1333 fps, and a FOV of  $102 \times 102 \mu\text{m}^2$ . Experimental observations of the Brownian motion of fluorescent microspheres and the photobleaching of fluorescently labeled microtubules in NIH/3T3 cells using our SIM system demonstrated its superiority over conventional SIM. With its outstanding performance, this proposed SIM technique holds great promise for applications in biomedical research, including the studies of organelle interactions [40], intracellular transport [41], and neuronal activity [42]. Moreover, this SIM technique can be readily applied to 3D SIM [43,44] by modifying the illumination patterns and reconstruction algorithm. The high-speed, large FOV, and super-resolution 3D imaging capabilities offered by this approach open up new possibilities for biological imaging. With the advancement of electronics, high-speed cameras with higher frame rates and large pixel counts have become available. Thus, the imaging speed and FOV of our SIM system can be further improved. However, it should be noted that the rolling reconstruction strategy only increases the overall frame rate and does not increase the temporal resolution for super-resolution features [45]. Besides, like other high-speed fluorescence microscopy techniques, this SIM technique faces the challenge of decreased SNR due to the limited number of photons captured during short exposure time, which can result in significant artifacts and reduced resolution in the reconstructed super-resolution images. Addressing this challenge necessitates the use of fluorescent labels with higher quantum efficiency and photochemical stability, along with reconstruction algorithms that possess high noise resistance.



**Funding.** National Natural Science Foundation of China (12325408, 12274129, 12374274, 12274139, 62105101, 62175066, 92150102, 12074121, 92150301, 12304338); Science and Technology Commission of Shanghai Municipality (21XD1400900); Fundamental Research Funds for the Central Universities.

**Disclosures.** The authors declare no conflicts of interest.

**Data availability.** Data underlying the results presented in this paper are not publicly available at this time but may be obtained from the authors upon reasonable request.

## Reference

1. B. Huang, M. Bates, and X. Zhuang, "Super-resolution fluorescence microscopy," *Annu. Rev. Biochem.* **78**(1), 993–1016 (2009).
2. L. Schermelleh, R. Heintzmann, and H. Leonhardt, "A guide to super-resolution fluorescence microscopy," *J. Cell Biol.* **190**(2), 165–175 (2010).
3. S. W. Hell and J. Wichmann, "Breaking the diffraction resolution limit by stimulated emission: stimulated-emission-depletion fluorescence microscopy," *Opt. Lett.* **19**(11), 780–782 (1994).
4. H. Blom and J. Widengren, "Stimulated emission depletion microscopy," *Chem. Rev.* **117**(11), 7377–7427 (2017).
5. M. J. Rust, M. Bates, and X. Zhuang, "Sub-diffraction-limit imaging by stochastic optical reconstruction microscopy (STORM)," *Nat. Methods* **3**(10), 793–796 (2006).
6. S. Manley, J. M. Gillette, G. H. Patterson, *et al.*, "High-density mapping of single-molecule trajectories with photoactivated localization microscopy," *Nat. Methods* **5**(2), 155–157 (2008).
7. M. G. L. Gustafsson, "Surpassing the lateral resolution limit by a factor of two using structured illumination microscopy," *J. Microsc.* **198**(2), 82–87 (2000).
8. R. Heintzmann and T. Huser, "Super-resolution structured illumination microscopy," *Chem. Rev.* **117**(23), 13890–13908 (2017).
9. F. Balzarotti, Y. Eilers, K. C. Gwosch, *et al.*, "Nanometer resolution imaging and tracking of fluorescent molecules with minimal photon fluxes," *Science* **355**(6325), 606–612 (2017).
10. M. Weber, M. Leutenegger, S. Stoldt, *et al.*, "MINSTED fluorescence localization and nanoscopy," *Nat. Photonics* **15**(5), 361–366 (2021).
11. S. C. M. Reinhardt, L. A. Masullo, I. Baudrexel, *et al.*, "Ångström-resolution fluorescence microscopy," *Nature* **617**(7962), 711–716 (2023).
12. M. G. L. Gustafsson, "Nonlinear structured-illumination microscopy: wide-field fluorescence imaging with theoretically unlimited resolution," *Proc. Natl. Acad. Sci. USA* **102**(37), 13081–13086 (2005).
13. E. H. Rego, L. Shao, J. J. Macklin, *et al.*, "Nonlinear structured-illumination microscopy with a photoswitchable protein reveals cellular structures at 50-nm resolution," *Proc. Natl. Acad. Sci. U. S. A.* **109**(3), E135–E143 (2012).
14. W. Zhao, S. Zhao, L. Li, *et al.*, "Sparse deconvolution improves the resolution of live-cell super-resolution fluorescence microscopy," *Nat. Biotechnol.* **40**(4), 606–617 (2022).
15. Y. He, Y. Yao, Y. He, *et al.*, "Surpassing the resolution limitation of structured illumination microscopy by an untrained neural network," *Biomed. Opt. Express* **14**(1), 106–117 (2023).
16. Y. He, Y. Yao, Y. He, *et al.*, "Untrained neural network enhances the resolution of structured illumination microscopy under strong background and noise levels," *Adv. Photonics Nexus* **2**(04), 046005 (2023).
17. F. Orieux, E. Sepulveda, V. Lorient, *et al.*, "Bayesian estimation for optimized structured illumination microscopy," *IEEE Trans. Image Process.* **21**(2), 601–614 (2012).
18. A. Lal, C. Shan, K. Zhao, *et al.*, "A frequency domain SIM reconstruction algorithm using reduced number of images," *IEEE Trans. Image Process.* **27**(9), 4555–4570 (2018).
19. S. Dong, J. Liao, K. Guo, *et al.*, "Resolution doubling with a reduced number of image acquisitions," *Biomed. Opt. Express* **6**(8), 2946–2952 (2015).
20. F. Ströhl and C. F. Kaminski, "Speed limits of structured illumination microscopy," *Opt. Lett.* **42**(13), 2511–2514 (2017).
21. Y. He, Y. Yao, D. Qi, *et al.*, "High-speed super-resolution imaging with compressive imaging-based structured illumination microscopy," *Opt. Express* **30**(9), 14287–14299 (2022).
22. Z. Huang, Y. Yao, Y. He, *et al.*, "Faster structured illumination microscopy using complementary encoding-based compressive imaging," *Photonics Res.* **12**(4), 740–748 (2024).
23. Y. He, Y. Yao, D. Qi, *et al.*, "Temporal compressive super-resolution microscopy at frame rate of 1200 frames per second and spatial resolution of 100 nm," *Adv. Photonics* **5**(02), 026003 (2023).
24. J. Park, D. J. Brady, G. Zheng, *et al.*, "Review of bio-optical imaging systems with a high space-bandwidth product," *Adv. Photonics* **3**(4), 044001 (2021).
25. F. Wang, L. Liu, H. Yu, *et al.*, "Scanning superlens microscopy for non-invasive large field-of-view visible light nanoscale imaging," *Nat. Commun.* **7**(1), 13748 (2016).
26. J. Fan, J. Suo, J. Wu, *et al.*, "Video-rate imaging of biological dynamics at centimetre scale and micrometre resolution," *Nat. Photonics* **13**(11), 809–816 (2019).
27. Y. Tochigi, K. Hanzawa, Y. Kato, *et al.*, "A global-shutter CMOS image sensor with readout speed of 1-Tpixel/s burst and 780-Mpixel/s continuous," *IEEE J. Solid-State Circuits* **48**(1), 329–338 (2013).

28. G. Wen, S. Li, L. Wang, *et al.*, “High-fidelity structured illumination microscopy by point-spread-function engineering,” *Light: Sci. Appl.* **10**(1), 70 (2021).
29. X. Huang, J. Fan, L. Li, *et al.*, “Fast, long-term, super-resolution imaging with Hessian structured illumination microscopy,” *Nat. Biotechnol.* **36**(5), 451–459 (2018).
30. D. Ulyanov, A. Vedaldi, and V. Lempitsky, “Deep image prior,” in *Proceedings of the IEEE conference on Computer Vision and Pattern Recognition*, (IEEE, 2018), pp. 9446–9454.
31. T. Li, S. Kheifets, D. Medellin, *et al.*, “Measurement of the instantaneous velocity of a Brownian particle,” *Science* **328**(5986), 1673–1675 (2010).
32. P. N. Pusey, “Brownian motion goes ballistic,” *Science* **332**(6031), 802–803 (2011).
33. R. Kubo, “Brownian motion and nonequilibrium statistical mechanics,” *Science* **233**(4761), 330–334 (1986).
34. R. D. Astumian, “Thermodynamics and kinetics of a Brownian motor,” *Science* **276**(5314), 917–922 (1997).
35. G. K. Batchelor, “Brownian diffusion of particles with hydrodynamic interaction,” *J. Fluid Mech.* **74**(1), 1–29 (1976).
36. A. P. Demchenko, “Photobleaching of organic fluorophores: quantitative characterization, mechanisms, protection,” *Methods Appl. Fluoresc.* **8**(2), 022001 (2020).
37. S. Zaiba, F. Lerouge, A.-M. Gabudean, *et al.*, “Transparent plasmonic nanocontainers protect organic fluorophores against photobleaching,” *Nano Lett.* **11**(5), 2043–2047 (2011).
38. S. J. M. Nassar, C. Wills, and A. Harriman, “Inhibition of the photobleaching of methylene blue by association with urea,” *ChemPhotoChem* **3**(10), 1042–1049 (2019).
39. N. Banterle, K. H. Bui, E. A. Lemke, *et al.*, “Fourier ring correlation as a resolution criterion for super-resolution microscopy,” *J. Struct. Biol.* **183**(3), 363–367 (2013).
40. D. Li, L. Shao, B.-C. Chen, *et al.*, “Extended-resolution structured illumination imaging of endocytic and cytoskeletal dynamics,” *Science* **349**(6251), aab3500 (2015).
41. R. Chen, X. Tang, Y. Zhao, *et al.*, “Single-frame deep-learning super-resolution microscopy for intracellular dynamics imaging,” *Nat. Commun.* **14**(1), 2854 (2023).
42. R. Turcotte, Y. Liang, M. Tanimoto, *et al.*, “Dynamic super-resolution structured illumination imaging in the living brain,” *Proc. Natl. Acad. Sci. USA* **116**(19), 9586–9591 (2019).
43. L. Shao, P. Kner, E. H. Rego, *et al.*, “Super-resolution 3D microscopy of live whole cells using structured illumination,” *Nat. Methods* **8**(12), 1044–1046 (2011).
44. L. Schermelleh, P. M. Carlton, S. Haase, *et al.*, “Subdiffraction multicolor imaging of the nuclear periphery with 3D structured illumination microscopy,” *Science* **320**(5881), 1332–1336 (2008).
45. A. Boualam and C. J. Rowlands, “Method for assessing the spatiotemporal resolution of structured illumination microscopy (SIM),” *Biomed. Opt. Express* **12**(2), 790–801 (2021).